Improving the Efficiency of Top-emitting AlGaN Nanowire Photonic Crystal Laser by Structural Modification

Dishiti Gupta, Tron Arne Nilsen, Bjørn-Ove Fimland, Helge Weman
[1]Department of Electronic Systems, Norwegian University of Science and Technology, 7491 Trondheim, Norway
dishiti.gupta@ntnu.no

***Abstract*—Nanowire (NW) based photonic crystal (PhC) structures have gained interest for top-emitting lasers in the UV region due to their lower defect density, ease of fabrication, better mode confinement due to higher refractive index contrast, and improved light extraction. We demonstrate the use of the finite difference time domain (FTDT) method to calculate the out-of-plane losses for passive PhC-based laser structures. An anti-taper is introduced in the lower part of the NW as a structural modification which improves the Q-factor and power output of the NW PhC laser structure.**

***Index Terms*—simulation, nanowire, photonic crystal, top-emitting laser.**

I. Introduction

The inherent germicidal properties of ultraviolet (UV) light make UV lasers important for sterilization, disinfection of water, air, or surfaces, and medical procedures [1]. Currently, only light-emitting diodes (LEDs) are available but lasers are highly desirable due to their higher power density. In top-emitting laser diodes, the light is emitted perpendicular to the substrate surface, allowing easier integration with optical components. Heterostructured nanowires (NWs) have reduced dimensional constraints compared to thin films or bulk materials, which leads to lower defect density and hence higher efficiency in devices such as NW lasers. Compared to etched thin film photonic crystal (PhC), the NW PhC avoids thin-film related defects and problems with high aspect ratio etching [2]. The PhCs formed by NWs have high refractive index contrast, leading to higher confinement and improved light extraction efficiency. This makes NW-based PhCs excellent candidates for top-emitting UV lasers. However, there is a lack of studies on structural modifications to increase the efficiency and light output for top-emitting NW-based laser structures. Here, we present simulation results from structural modification of NW-based PhC structure which can lead to increased efficiency and light output for a top-emitting laser.

II. Simulation Method

We use the open-source MIT Electromagnetic Equation Propagation (MEEP) software to model a top-emitting AlGaN NW-based PhC laser structure [3]. The finite-difference time-domain (FDTD) method is used to acquire the optical field profile, the top flux (the percentage of energy coupled out of the top of PhC relative to the sum of the top and bottom), and the time-dependent decay. The Q-factor is the number of cycles it takes for the energy stored in a resonator to decay to $1/e$ times its initial value [4]. The computational model is designed to account for the out-of-plane losses for a passive structure since the material losses are highly dependent on the physical structure itself [5]. The NW structure (Fig.1), is placed on a 2 μm n-GaN layer representing the top layer of the n-GaN on sapphire substrate. A thin hole-patterned TiN layer is incorporated in the structure as a growth mask [6]. For ease of simulation, we use a cylindrical NW compared to more complex shapes like hexagonal NW. The effective refractive index for the NW structure is 2.57.

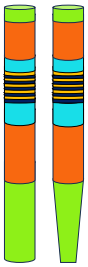

(a)

Layer	Thickness [nm]	Refractive index [n]
p-GaN	30	2.65
p-$Al_{0.2}Ga_{0.8}N$	250	2.57
p-$Al_{0.09}Ga_{0.91}N$	60	2.61
5 GaN/$Al_{0.09}Ga_{0.91}N$ QWs	30	2.62
n-$Al_{0.09}Ga_{0.91}N$	40	2.61
n-$Al_{0.2}Ga_{0.8}N$	400	2.57
n-GaN	600	2.65

(b)

Fig. 1: (a) Schematic diagram of a NW without anti-taper (left) and a NW with anti-taper (right) with the designed GaN/AlGAN NW layer structure. (b) Thickness [6] and refractive index (n) [7], [8] of the different GaN/AlGaN layers of the NW

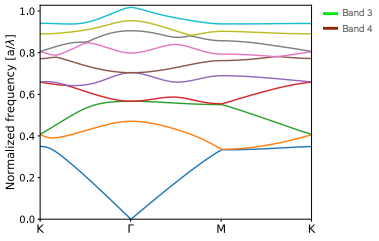

Fig. 2: Band structure of the designed NW PhC structure targeted to operate at $a/\lambda = 0.567$ with nanowire radius $(r) = 0.4a$

We simulate a triangular lattice PhC with a lattice constant (a) of 207 nm and NW radius (r) of 83 nm ($r = 0.4a$). $r = 0.455a$ used in [6] makes it difficult to achieve high refractive index contrast and leads to narrow bandgaps due to lower mode confinement in the quantum well (QW) core region of the NW waveguides and difficulty in achieving a standing wave formation [9] in the PhC with large r/a value. At the same time, a low r/a value provides a high refractive

index contrast but reduces the area of the gain material, leading to lower gain at the same inversion density for the PhC laser structure. Therefore, $r = 0.4a$ was chosen for our simulations. Fig. 2 shows the band diagram for transverse electric (TE) polarization (magnetic field along the c-axis of the NW). TE polarization was used for the simulations as it is the dominant polarization in c-oriented GaN/AlGaN QW structures [10]. The normalized frequency a/λ of the NW PhC is 0.567, corresponding to the degenerate bands 3 and 4 close to the Γ point.

III. Results and Discussion

The optical field profile illustrated in Fig. 3 for NW PhC without anti-taper (Cylinder), indicates high field leakage into the substrate (white region below the bottom of NW), leading to losses, a low Q-factor of 613, and a poor top flux of 2.2% (Table II). The mode is not well confined in the core (yellow region) of the NW. A high degree of overlap between the QWs present in the core and the mode is necessary for an efficient low-threshold laser [11].

TABLE II: Effect of different NW geometries on the mode wavelength, top flux, Q-factor and total loss (total loss $= 2\pi/(\text{Q-factor} \times a)$ for band-edge modes of band 3 and 4. M1 and M2 correspond to the two modes at the band edge of bands 3 and 4. "S" represents the shortened NW where both the n-GaN and the n-$Al_{0.2}Ga_{0.8}N$ layer thicknesses are reduced to 200 nm.

Structure	Modes	Wavelength [nm]	Top flux [%]	Q-factor	Total loss [cm^{-1}]
Cylinder NW	M1	366.07	2.2	613	495
Anti-taper NW	M1	366.00	37.6	27153	11.2
Anti-taper NW	M2	366.33	15.7	24710	12.3
S-Cylinder NW	M1	371.19	0.6	323	938
S-Anti-taper NW	M1	365.93	12.0	15067	20.1
S-Anti-taper NW	M2	366.81	11.6	2421	125

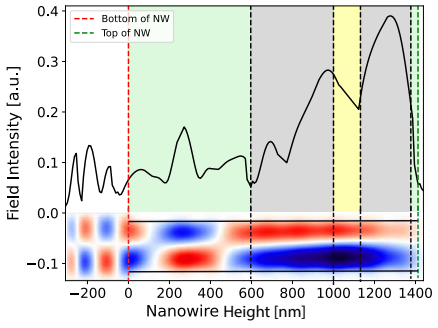

Fig. 3: TE mode field intensity profile of the magnetic field component in NW axial direction for the NW without anti-taper, called "Cylinder NW"

To confine the mode to the core, an anti-taper was introduced at the n-GaN layer (Anti-taper). This reduces the effective index of the lower part of the NW waveguide and pushes the mode into the core, reducing the losses into the substrate as illustrated in Fig. 4. This increases the Q-factors to 27153 and 24710, as well as the outcoupling fluxes to 37.6% and 15.7%, for the band-edge modes at band 3 and 4, respectively. The total losses are reduced from 495 cm^{-1} in the cylindrical NW to 12.3 cm^{-1} and 11.2 cm^{-1} in the anti-tapered NWs. The splitting of the degenerate modes 3 and 4 can be an artifact of the discretization of the simulation.

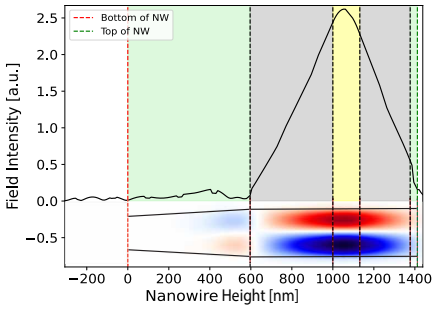

Fig. 4: TE mode field intensity profile of the magnetic field component in NW axial direction for the "Anti-taper NW"

In practice, it is convenient to manufacture a shorter NW. Hence, we shorten the NW by reducing the length of the n-GaN and the n-$Al_{0.2}Ga_{0.8}N$ layers to 200 nm each. This makes the NW structure very leaky but, again introducing an anti-taper improves the leaky behavior and leads to a higher top flux as depicted in Table II.

IV. Conclusion

In conclusion, we have increased the Q-factor by a factor of 44 to 27153 and the top flux from 2.2% to 37.6% in a top-emitting AlGaN NW PhC laser structure by introducing an anti-taper in the bottom n-GaN NW layer. For a shortened NW structure a similar effect was observed. The Q-factor improved by a factor of 47 to 15067 and the top flux from 0.6% to 12%. Hence, the anti-tapering helps to confine the mode in the core, reducing the losses to the substrate and leading to improvements in the Q factor and top emission flux.

References

[1] K. Song, M. Mohseni, and F. Taghipour, "Application of ultraviolet light-emitting diodes (UV-LEDs) for water disinfection: A review," *Water Research*, vol. 94, pp. 341–349, 2016.

[2] M. H. Huang, S. Mao, H. Feick, H. Yan, Y. Wu, H. Kind, E. Weber, R. Russo, and P. Yang, "Room-Temperature Ultraviolet Nanowire Nanolasers," *Science*, vol. 292, no. 5523, pp. 1897–1899, 2001.

[3] A. F. Oskooi, D. Roundy, M. Ibanescu, P. Bermel, J. Joannopoulos, and S. G. Johnson, "Meep: A flexible free-software package for electromagnetic simulations by the FDTD method," *Computer Physics Communications*, vol. 181, pp. 687–702, 2010.

[4] B. Saleh and M. Teich, *Fundamentals of Photonics, 3rd Edition*. John Wiley & Sons, Ltd, 2019.

[5] W.-H. Hsieh, D.-H. Huang, T.-C. Chen, P.-Y. Chang, T.-C. Lu, and C.-Y. Huang, "Optimal waveguide structure for low-threshold InGaN/GaN-based photonic-crystal surface-emitting lasers," *AIP Advances*, vol. 14, no. 4, p. 045108, 2024.

[6] B. H. Le, X. Liu, N. H. Tran, S. Zhao, and Z. Mi, "An electrically injected AlGaN nanowire defect-free photonic crystal ultraviolet laser," *Optics Express*, vol. 27, pp. 5843–5850, Feb. 2019.

[7] E. D. Palik, *Handbook of Optical Constants of Solids*. Academic Press, 1998.

[8] M. N. Polyanskiy, "Refractiveindex.info database of optical constants," *Scientific Data*, vol. 11, p. 94, 2024.

[9] J. D. Joannopoulos, S. G. Johnson, J. N. Winn, and R. D. Meade, *Photonic crystals: molding the flow of light*. Princeton University Press, 2nd ed., 2008.

[10] R. G. Banal, M. Funato, and Y. Kawakami, "Optical anisotropy in [0001]-oriented $Al_xGa_{1-x}N$/AlN quantum wells ($x > 0.69$)," *Physical Review B*, vol. 79, no. 12, p. 121308, 2009.

[11] A. Ghadimi and S. Alikhah, "Simulation and analysis of dependence of threshold current and gain of $\lambda/4$ shifted DFB laser through transfer matrix," *Journal of Optics*, vol. 46, no. 4, pp. 479–485, 2017.